Combined LEGO-eigencurrent approach for enhanced solution of electrically large 2-D EBG structures

Combined LEGO-Eigencurrent Approach For Enhanced Solution of Electrically Large 2-D EBG Structures

D.Duque*, V.Lancellotti*, B.P de Hon*
*Department of Electrical Engineering, Eindhoven University of Technology
Den Dolech P.O. Box 513, 5600 MB, Eindhoven, The Netherlands
d.j.duque@tue.nl

***Abstract*—We combine the linear embedding via Green's operators (LEGO) and the eigencurrent expansion method (EEM) to efficiently deal with 2-D electrically large electromagnetic band-gap (EBG) structures. In LEGO, the composite structure is broken up into elements called "bricks" that are characterized through *scattering operators* by invoking *Love's equivalence principle*. The problem is then formulated through an integral equation involving the *total inverse scattering operator* $\mathcal{S}^{-1}$ of the structure. The resulting equation is solved by the method of moments (MoM) and the EEM, which allows for considerable reduction in the size of the resulting MoM matrix. Therefore, it enables us to handle relatively large structures.**

I. Introduction

Over the past decades electromagnetic band-gap (EBG) structures have drawn significant attention in physics and engineering communities because they allow for more control of the propagation of electromagnetic waves. Several approaches have been used in order to analyse such structures. The plane-wave method has been used extensively for the analysis of fully periodic structures [1]. A variety of transfer-matrix methods have been developed [2], [3]. These methods are more flexible than the plane-wave method, in that periodicity is no longer required in one direction. Nevertheless, transfer-matrix methods are not inherently stable. The scattering matrix method [4] has been used to analyse periodic structures composed of multiple layers of frequency selective surfaces (FSS). The method (originated from that of cascading networks in circuit theory) considerably reduces the computing time as compared to conventional methods which calculate the overall scattering from the structure. The finite difference time domain (FDTD) method is also commonly used to optimize and compute band-gap diagrams for photonic crystals (PhC) and 2-D metal photonic band-gap cavities [5]. On the other hand, when a numerical solution is contemplated either in the spatial, temporal or spectral domain by means of the Finite Element Method (FEM) [6], the FDTD [7] or the method of moments (MoM)[8], the issue of storing and formally inverting the system matrix or refining the FDTD grid may become computationally demanding.

As an alternative to the numerical methods outlined above, in [9] a diakoptic approach [10], called linear embedding via Green's operators (LEGO) was proposed to analyse 2-D EBG devices. In LEGO, the first step toward the solution is to embed each object forming the EBG device within a bounded domain (dubbed "brick"). Then, each brick is characterized by its scattering operator. Finally, in [9] the scattering operators were combined in a cascade of succesive embedding steps to obtain the total scattering operator of the structure. The main drawback of this approach is that the intermediate scattering matrices grow considerably with each iteration step, causing a rapid drain of memory resources and consequently limiting the number of interacting domains that can be handled.

In order to circumvent these difficulties, we combine LEGO with the eigencurrent expansion method (EEM) as in [11]. Among the reasons to support the aforementioned extension to the 2-D instance, we mention:

- Many EBG structures providing band-gap field confinement in the optical or microwave frequency range may be well approximated as 2-D geometries.
- In 2-D geometries, the fields can be decomposed into two orthogonal polarisations, which renders the problem much "cleaner" and easier to analyse.
- EBG structures, especially those encountered in optics, may allow for a 2.5-D analysis which is a natural extension of the 2-D case. In a 2.5-D analysis, many of the 2-D characteristics of the problem are preserved while the excitation is in part extended to the 3-D case, as for example a plane wave at oblique incidence.

This paper is organized as follow: In Section II, we introduce the notion of LEGO brick and we define its scattering operator. In Section III, we formulate the EM problem of an EBG structure in terms of the inverse scattering operator $\mathcal{S}^{-1}$. In Section IV, we describe the EEM and in Section V, we present numerical results for the implemented approach.

II. Definition of a LEGO brick and its scattering operator

We consider an EBG structure comprised of N_B identical elements which are immersed in a homogeneous background medium. In LEGO [9], [11] we start solving the problem by "tearing apart" the structure into its constituent elements, as also done in [12], [13] for antenna problems. We then embed each element in a bounded domain $\mathcal{D}_k,\ k = 1, \cdots, N_B$, as shown in Fig.1. We refer to $\mathcal{D}_k$ as LEGO *brick* and we characterize it electromagnetically by means of a *scattering*

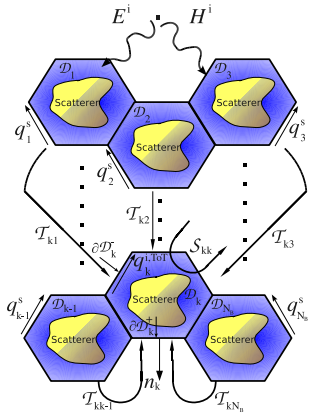

Figure 1. The LEGO concept: A large 2-D structure is divided into small subdomains, and each of them is characterized by its own scattering operator $\mathcal{S}_{kk}$.The multiple scattering taking place in the structure is accounted for by the transfer operators $\mathcal{T}_{kn}$.

operator $\mathcal{S}_{kk}$. Which links equivalent incident currents to equivalent scattered currents. To derive $\mathcal{S}_{kk}$, let us consider the problem of just one brick $\mathcal{D}_k$ (see Fig.1). This brick is illuminated by an arbitrary incident fields $\boldsymbol{F^i}$ and, since an object is embedded in it, scattered fields $\boldsymbol{F^s}$ are excited. $\boldsymbol{F^s}$ can be regarded as being produced by equivalent sources $\boldsymbol{q_o}$ on the object surface $\partial\mathcal{D}_o$. More precisely, we define

$$\boldsymbol{F^i} = \begin{bmatrix} \boldsymbol{E^i} \\ \boldsymbol{H^i} \end{bmatrix}, \qquad \boldsymbol{F^s} = \begin{bmatrix} \boldsymbol{E^s} \\ \boldsymbol{H^s} \end{bmatrix}, \tag{1}$$

where we assume a time-harmonic dependence $\exp(\jmath\omega t)$ throughout. By invoking *Love's equivalence principle* [14], an observer inside $\mathcal{D}_k$ can not distinguish between the field $\boldsymbol{F^i}$ excited by the actual sources outside $\mathcal{D}_k$ and a carefully constructed distribution of equivalent surface sources $\boldsymbol{q_k^i}$ on $\partial\mathcal{D}_k^+$. Conversely, an observer outside $\mathcal{D}_k$ can not distinguish between the field $\boldsymbol{F^s}$ excited by $\boldsymbol{q_o}$ inside $\mathcal{D}_k$ and a carefully constructed distribution of equivalent surface sources $\boldsymbol{q_k^s}$ on $\partial\mathcal{D}_k^-$. These quantities are defined as

$$\boldsymbol{q_k^i} = \begin{bmatrix} \boldsymbol{J_k^i} \\ \boldsymbol{M_k^i} \end{bmatrix}, \qquad \boldsymbol{q_k^s} = \begin{bmatrix} \boldsymbol{J_k^s} \\ \boldsymbol{M_k^s} \end{bmatrix}, \qquad \boldsymbol{q_o} = \begin{bmatrix} \boldsymbol{J_o} \\ \boldsymbol{M_o} \end{bmatrix}, \tag{2}$$

where $\boldsymbol{J}$ and $\boldsymbol{M}$ are electric and magnetic current densities. Love's equivalence principle states that the current densities $\boldsymbol{q_k^{i,s}}$ are the tangential components of the fields $\boldsymbol{F^{i,s}}$ on either side of $\partial\mathcal{D}_k$, viz.

$$\boldsymbol{q_k^i} = \begin{bmatrix} -\boldsymbol{n_k} \times \boldsymbol{H_k^i} \\ -\boldsymbol{E_k^i} \times \boldsymbol{n_k} \end{bmatrix}, \qquad \boldsymbol{q_k^s} = \begin{bmatrix} \boldsymbol{n_k} \times \boldsymbol{H_k^s} \\ \boldsymbol{E_k^s} \times \boldsymbol{n_k} \end{bmatrix}, \tag{3}$$

which provides a means to compute $\boldsymbol{q_k^{i,s}}$. Nevertheless, we prefer to determine $\boldsymbol{q_k^{i,s}}$ through two BIEs posed on $\partial\mathcal{D}_k$ using the so called *propagators* [11], namely

$$\mathcal{P}_{kk}^i \boldsymbol{q_k^i} = \int_{\partial\mathcal{D}_k^+} P_{kk}^i(\boldsymbol{\rho},\boldsymbol{\rho'})\boldsymbol{q_k^i}(\boldsymbol{\rho'})\mathrm{d}C' = \boldsymbol{F_{tk}^i}, \quad \boldsymbol{\rho} \in \partial\mathcal{D}_k^+, \tag{4}$$

$$\mathcal{P}_{kk}^s \boldsymbol{q_k^s} = \int_{\partial\mathcal{D}_k^-} P_{kk}^s(\boldsymbol{\rho},\boldsymbol{\rho'})\boldsymbol{q_k^s}(\boldsymbol{\rho'})\mathrm{d}C' = \boldsymbol{F_{tk}^s}, \quad \boldsymbol{\rho} \in \partial\mathcal{D}_k^-, \tag{5}$$

where $\boldsymbol{F_{tk}^{i,s}}$ are the tangential components of $\boldsymbol{F^{i,s}}$ on $\partial\mathcal{D}_k^{\pm}$ and $P_{kk}^{i,s}(\boldsymbol{\rho},\boldsymbol{\rho'})$ are 2×2 matrices whose entries are dyadic integro-differential operators involving the 2-D scalar Green's function $K_o(\gamma|\boldsymbol{\rho}-\boldsymbol{\rho'}|)$. The reason why (4)-(5) are prefered to calculate $\boldsymbol{q_k^{i,s}}$ is that, although the identity operator associated with (3) is easy to discretize, in (3) an integral operator with highly singular kernel is also implied, which leads to slow convergence rates in conjuction with the MoM [15].

We are now able to introduce the scattering operator $\mathcal{S}_{kk}$ on $\partial\mathcal{D}_k$ as

$$\boldsymbol{q_k^s} = \mathcal{S}_{kk}\boldsymbol{q_k^i} = \int_{\partial\mathcal{D}_k^+} S_{kk}(\boldsymbol{\rho},\boldsymbol{\rho'})\boldsymbol{q_k^i}(\boldsymbol{\rho'})\mathrm{d}C', \quad \boldsymbol{\rho} \in \partial\mathcal{D}_k^-, \tag{6}$$

where we see that $\mathcal{S}_{kk}$ maps equivalent incident currents to equivalent scattered currents on either side of $\partial\mathcal{D}_k$. In order to deduce an expression for $\mathcal{S}_{kk}$, we must solve the scattering problem inside $\mathcal{D}_k$. This calculation implies a BIE of the form

$$\mathcal{X}_{oo}\boldsymbol{q_o} = \boldsymbol{F_{to}^i}, \tag{7}$$

where $\mathcal{X}_{oo}$ will depend on the adopted formulation (e.g., the EFIE, MFIE or CFIE [16] for perfect electric conductors (PEC) and the PMCHWTS [16] or Müller [17] for homogeneous penetrable objects) and the tangential field $\boldsymbol{F_{to}^i}$ on $\partial\mathcal{D}_o$ is given by

$$\boldsymbol{F_{to}^i} = \mathcal{P}_{ok}\boldsymbol{q_k^i} = \int_{\partial\mathcal{D}_k^+} P_{ok}(\boldsymbol{\rho},\boldsymbol{\rho'})\boldsymbol{q_k^i}(\boldsymbol{\rho'})\mathrm{d}C', \quad \boldsymbol{\rho} \in \partial\mathcal{D}_o. \tag{8}$$

Similarly, we obtain $\boldsymbol{F_{tk}^s}$ from $\boldsymbol{q_o}$ by applying a propagator $\mathcal{P}_{ko}$ from $\partial\mathcal{D}_o$ to $\partial\mathcal{D}_k^-$, viz.,

$$\boldsymbol{F_{tk}^s} = \mathcal{P}_{ko}\boldsymbol{q_o} = \int_{\partial\mathcal{D}_o} P_{ko}(\boldsymbol{\rho},\boldsymbol{\rho'})\boldsymbol{q_o}(\boldsymbol{\rho'})\mathrm{d}C', \quad \boldsymbol{\rho} \in \partial\mathcal{D}_k^-. \tag{9}$$

Finally, with (5) and upon eliminating $\boldsymbol{q_o}$, $\boldsymbol{F_{to}^i}$ and $\boldsymbol{F_{tk}^s}$ from (7), (8) and (9), we find the following expresion for $\mathcal{S}_{kk}$

$$\mathcal{S}_{kk} = (\mathcal{P}_{kk}^s)^{-1}\mathcal{P}_{ko}(\mathcal{X}_{oo})^{-1}\mathcal{P}_{ok}. \tag{10}$$

Note that $\mathcal{S}_{kk}$ depends on the content of $\mathcal{D}_k$ through $(\mathcal{X}_{oo})^{-1}$ and on the shape of $\partial\mathcal{D}_k$ through the propagators.

III. The Total Inverse Scattering Operator

Observe that we are more interested in computing $\boldsymbol{q_k^s}$ over the bricks rather than the total scattering operator $\mathcal{S}$ of the structure. Therefore, we formulate the problem in terms of an equation to be solved for $\boldsymbol{q_k^s}$. In particular, $\boldsymbol{q_k^s}$ still follows from (6) provided we include in the equivalent incident current the contribution of the remaining $N_B - 1$ bricks. This reads

$$\boldsymbol{q_k^s} = \mathcal{S}_{kk}\boldsymbol{q_{k,tot}^i} = \mathcal{S}_{kk}\left(\boldsymbol{q_k^i} + \sum_{n\neq k}\boldsymbol{q_{k(n)}^i}\right),\ \forall k, \tag{11}$$

where we express the contribution of the other bricks by means of *transfer operators* $\mathcal{T}_{kn}$ [9]-[11] (see Fig. 1), namely

$$\boldsymbol{q_{k(n)}^i} = \mathcal{T}_{kn}\boldsymbol{q_n^s} = \int_{\partial\mathcal{D}_n^-} T_{kn}(\boldsymbol{\rho},\boldsymbol{\rho'})\boldsymbol{q_n^s}(\boldsymbol{\rho'})\mathrm{d}C',\ \forall k\neq n. \tag{12}$$

The N_B BIEs implicitly stated in (11) can be formally solved for $\boldsymbol{q_k^s}$ in order to highlight the total inverse scattering operator, $\mathcal{S}^{-1}$, of the structure, i.e.,

$$\mathcal{S}^{-1}\boldsymbol{q^s} = \boldsymbol{q^i}, \tag{13}$$

with

$$\mathcal{S}^{-1} = \begin{bmatrix} \mathcal{S}_{11}^{-1} & -\mathcal{T}_{12} & \cdots & -\mathcal{T}_{1N_B} \\ -\mathcal{T}_{21} & \mathcal{S}_{22}^{-1} & \cdots & -\mathcal{T}_{2N_B} \\ \vdots & \vdots & \ddots & \vdots \\ -\mathcal{T}_{N_B1} & -\mathcal{T}_{N_B2} & \cdots & \mathcal{S}_{N_BN_B}^{-1} \end{bmatrix}, \tag{14}$$

$$\boldsymbol{q^s} = \begin{bmatrix} \boldsymbol{q_1^s} \\ \boldsymbol{q_2^s} \\ \vdots \\ \boldsymbol{q_{N_B}^s} \end{bmatrix}, \qquad \boldsymbol{q^i} = \begin{bmatrix} \boldsymbol{q_1^i} \\ \boldsymbol{q_2^i} \\ \vdots \\ \boldsymbol{q_{N_B}^i} \end{bmatrix}. \tag{15}$$

We see that (13), (14) and (15) constitutes the EM formulation of the problem in Fig. 1. In general we cannot invert (14) in close form, except when the structure is comprised of two bricks [9]. Hence, we apply the MoM and EEM in order to solve (13) efficiently.

IV. The Eigencurent Expansion Method

Let us assume that the the currents $\boldsymbol{q_k^{i,s}}$ on $\partial\mathcal{D}_k^{\pm}$ have been expanded using a set $\mathbb{B}_k$ of $2N_f$ basis functions on a regular mesh[1]. The idea behind the EEM is to expand $\boldsymbol{q^{i,s}}$ in (13) using a set $\mathbb{E}$ of functions that are *approximations* to the eigenfunctions of the operator $\mathcal{S}^{-1}$ [11]. We dub these functions *eigencurrents* because in the light of (13), $\mathcal{S}^{-1}$ maps currents to currents. To figure out what the set $\mathbb{E}$ should be, we neglect for a moment the multiple reflections taking place in the structure of Fig. 1. In this ideal case, the eigencurrents $\{\boldsymbol{e_m^{(k)}}\}$ of $\mathcal{S}^{-1}$ are formed by the juxtaposition of the eigencurrents $\{\boldsymbol{u_m^{(k)}}\}$ of $\mathcal{S}_{kk}$, viz.

$$\boldsymbol{e_m^{(k)}} = \left[\boldsymbol{0},\cdots,\boldsymbol{u_m^{(k)}},\cdots,\boldsymbol{0}\right]^t,\ m\in\mathbb{N}, \tag{16}$$

i.e., they are zero over all $\partial\mathcal{D}_n$, except on $\partial\mathcal{D}_k$ where they coincide with $\boldsymbol{u_m^{(k)}}$.

To apply the EEM to (13), we follow the procedure outlined in [11]. In this way (13) passes over to the following two uncoupled systems

$$\left[\check{S}_{\mathrm{cc}}\right]^{-1}\left[\check{q}_{\mathrm{c}}^s\right] = \left[\check{q}_{\mathrm{c}}^i\right],\quad \left[\Lambda_{\mathrm{uu}}\right]^{-1}\left[\check{q}_{\mathrm{u}}^s\right] = \left[\check{q}_{\mathrm{u}}^i\right], \tag{17}$$

[1]A regular mesh will prevent segments belonging to different boundaries from overlapping partially when any two bricks touch one another.

where $\left[\check{q}_{\mathrm{c,u}}^{i,s}\right]$ are the coefficients of the incident and scattered current expanded in terms of the *coupled* (*uncoupled*) eigencurrents. From (17) we see that we have turned the problem in (13) into the formal inversion of a diagonal matrix $\left[\Lambda_{\mathrm{uu}}\right]^{-1}$ plus the solution of a system whose matrix, $\left[\check{S}_{\mathrm{cc}}\right]^{-1}$, is far smaller than $[S]^{-1}$. Eventually, upon returning to the original basis $\bigcup\mathbb{B}_k$, we find

$$[q^s] \approx [G]\,[P]^t\begin{bmatrix}\left[\check{q}_{\mathrm{c}}^s\right] \\ \left[\check{q}_{\mathrm{u}}^s\right]\end{bmatrix}. \tag{18}$$

where P is a *permutation* matrix (with $[P]\,[P]^t = [I]$) which order the coefficients in $\left[\check{q}_{\mathrm{c,u}}^s\right]$ to form $[\check{q}^s]$ as in [11] and $[G]$ is a Gram matrix to pass from the eigencurrent basis to the original basis [11]. Equations (17), (18) have remarkable numerical features that are mentioned in [11].

V. Numerical Results

We have implemented the LEGO approach together with the EEM in a numerical code to handle arbitrary 2-D brick shapes enclosing either PEC or dielectric objects. To test the code, we first consider the scattering from an aggregate of 16 PEC cylinders (radius r) arranged in a square lattice, as shown in Fig. 2. Each cylinder is discretized with $N_o = 80$ edges and embedded in a square brick discretized with $N_f = 90$ edges. The relative size of the cylinders with respect to the bricks is $r/a = 0.25$ with $a = 1\,\mathrm{m}$. To represent the unknown current densities, we use triangular pulses as basis and test functions. A cylindric wave with TM polarization with respect to z and $f = 300\,\mathrm{MHz}$ is used to illuminate the array.

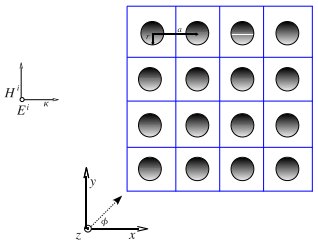

Figure 2. For LEGO-EEM validation: A composite structure of 16 2-D PEC cylinders embedded in square bricks.

Fig. 3 shows the computed bi-RCS obtained using the LEGO-EEM (-) with 21 *coupled* eigencurrents per brick, and direct MoM (applied to the CFIE($*$),MFIE($\diamondsuit$) and the EFIE($\square$)). As we can see, the bi-RCS predicted by all the methods are in excellent agreement, thus confirming the correctness of the LEGO-EEM approach. To give an idea of the gain in terms of memory, for the structure of Fig. 2. The size of the system to be solved shrinks down to $N_BN_c \times N_BN_c = 336\times 336$ in comparison to $N_BN_o \times N_BN_o = 1280\times 1280$ when using the MoM on the entire structure.

Next, we considerer a more elaborate numerical example, namely, a cylindrical EBG (CEBG) structure composed of concentric layers of metallic wires. Each metallic wire (radius

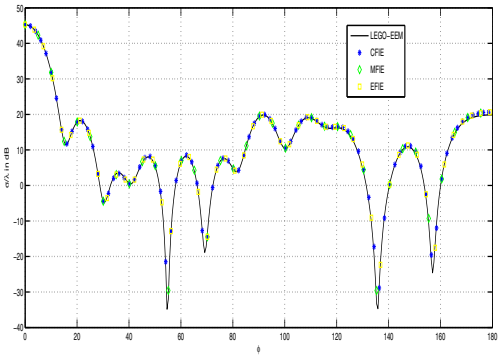

Figure 3. LEGO-EEM validation: The bi-RCS for the structure in Fig. 2; LEGO-EEM solution (-) vs CFIE (∗), MFIE (♢) and EFIE (□).

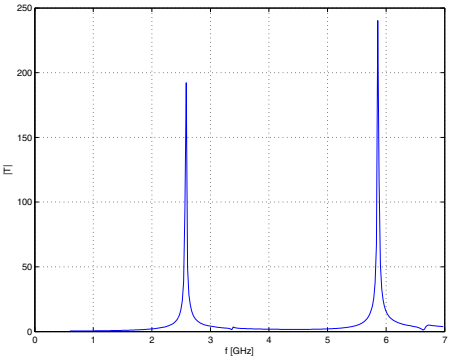

Figure 5. Transmission coefficient $|T|$ of the CEBG in Fig. 4.

a) is embedded in a square brick as shown in Fig.4. The

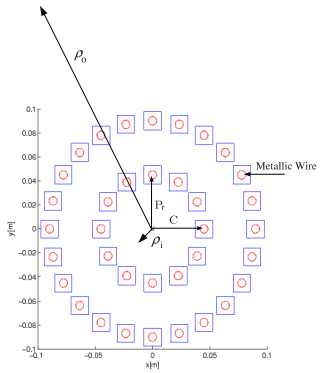

Figure 4. CEBG structure composed of concentric layers of metallic wires and LEGO model.

cylindrical layers are radially spaced with period $P_r = C$ and have the same transversal period $P_t = CP_\phi^k$. P_ϕ^k is the angular separation between any two neighboring wires in layer k, $k = 1, \cdots, N_L$ [18],[19]. The CEBG is illuminated by a line source with unit current amplitude placed at the center.

We assume $a = 3.5\,\text{mm}$, $C = P_r = 45\,\text{mm}$, $P_\phi^1 = \pi/6$, $N_L = 2$, $N_o = 50$ and $N_f = 44$. We compute the transmision coefficient T of the CEBG as a function of the frequency f. T is defined as the radiated transverse electric field outside the cavity at a point $\boldsymbol{\rho_o}$ normalized by the radiated field of the source alone. Fig. 5 shows the computed T. We observe as many resonances as the number of layers forming the CEBG [18],[19]. The reason why $|T|$ is greater than one at resonances is that the cavity improves the matching to free-space of the initially mismatched line source.

In order to study the focusing characteristics of the CEBG structure, We introduce defects in the CEBG by removing selected wires. Then, we compute the radiation pattern of the resulting structure using the same parameters as before. Two defective configuration with $N_L \in \{4, 6, 8, 10, 12, 14\}$ and $N_B \in \{1036, 826\}$ are considered, as illustrated in Figs. 6(a), 6(c). Figs. 6(b) and 6(d) show the radiation pattern in the H-plane at 2 GHz.

The directivity increases with the number of layers and the side-lobes level decreases correspondingly. The increase in the directivity can be explained by the widening of the effective area of the CEBG and the decrease in the side-lobes by the decrease in the magnitude of $|T|$ in the stop-band (band-gap) of the CEBG when the number of layers increases [18], [19].

Finally, to discuss the complexity of LEGO-EEM, in Table I we list the characteristic sizes of the problem in Fig. 6(a). If we compare the size $N_cN_B \times N_cN_B$ of $\left[\check{S}_{\text{cc}}\right]^{-1}$ with the size $N_oN_B \times N_oN_B$ of the problem solved using the MoM, then the efficiency of LEGO-EEM to handle large structures becomes evident.

Table I
CHARACTERISTIC SIZES OF THE PROBLEM AND MEMORY USAGE

$N_f = 44$, $N_o = 50$, $N_c = 18$					Memory [MB]	
N_L	N_B	$2N_fN_B$	N_oN_B	N_cN_B	$\left[\check{S}_{\text{cc}}\right]^{-1}$	BIE
4	96	8448	4800	1728	46	352
6	204	17952	10200	3672	206	1588
8	352	30976	17600	6336	613	4727
10	540	47520	27000	9720	1442	11124
12	768	67584	38400	13824	2916	22500
14	1036	91168	51800	18648	5306	40943

VI. CONCLUSIONS

We have combined the LEGO with the EEM for dealing with 2-D electrically large EBG structures. We have carried out two numerical examples in order to test the correctness and the efficiency of LEGO-EEM. In the first test, the computation of the bi-RCS shows that the LEGO-EEM is accurate when a small number of *coupled* eigencurrents is used to solve the electromagnetic problem. The second test has been carried out to verify the capabilities of LEGO-EEM to handle large structures.

ACKNOWLEDGMENTS

This research was supported by the MEMPHIS project under contract No 10006758.

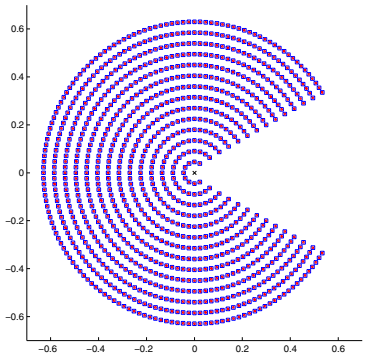

(a) CEBG with $N_L = 14$, $N_B = 1036$ LEGO bricks and defects by removing $3, 5, 7, 9, \cdots$ wires in each layer.

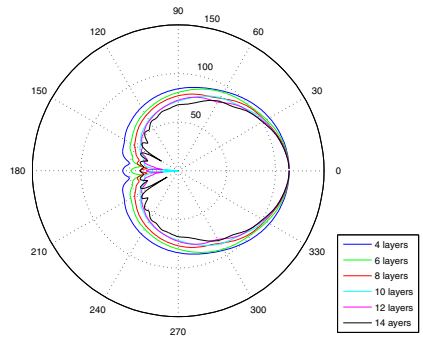

(b) Computed radiation pattern in the H-plane at 2 GHz as a function of the number of layer N_L.

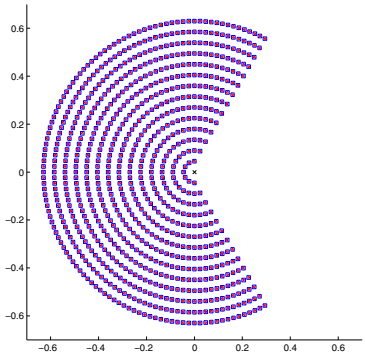

(c) CEBG with $N_L = 14$, $N_B = 826$ LEGO bricks and defects by removing $5, 9, 13, 17, \cdots$ wires in each layer.

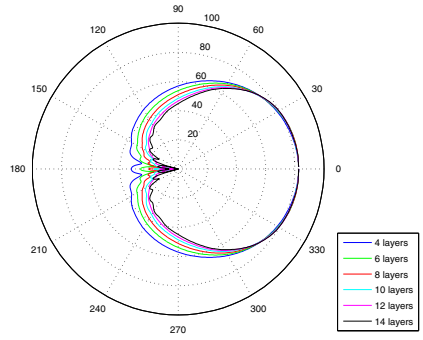

(d) Computed radiation pattern in the H-plane at 2 GHz as a function of the number of layer N_L.

Figure 6. Geometry of the CEBG with defects and $a = 3.5$ mm, $C = P_r = 45$ mm, $P_\phi^1 = \pi/6$ and radiation patterns as a function of N_L

REFERENCES

[1] K. Ho, C. Chan, and C. Soukoulis, "Existence of a photonic gap in periodic dielectric structures," *Physical Review Letters*, 1990.

[2] P. Bell, J. Pendry, L. Moreno, and A. Ward, "A program for calculating photonic band structures and transmision coefficients of complex structures," *Computer Physics Communications*, 1995.

[3] A. Reynolds, H. Chong, I. Thayne, J. Arnold, and P. de Maagt, "Angular frequency dependence for a planar cavity defect introduced into a 2-D dimensional photonic crystal," *IEEE Trans. Microwave Theory Tech.*, vol. 49, pp. 1254–1261, July 2001.

[4] R.C.Hall, R. Mittra, and K.M Mitzner, "Analysis of multilayered periodic structures using generalized scattering matrix," *IEEE Trans. Antennas Propagat.*, vol. 36, pp. 111–117, Apr. 1988.

[5] D. Smith, S. Schultz, and N. Kroll, "Experimental and theoritical results for two-dimensional metal photonic band-gap cavity," *Applied Physic. Letter. 65*, 1994.

[6] O. Zienkienwicz, *The Finite Element Method in Engineering Science*. London:McGraw-Hill, 1971.

[7] K. Yee, "Numerical solution of initial boundary value problems involving Maxwell's equations in isotropic media," *IEEE Trans. Antennas Propagat.*, vol. 14, pp. pp 302–307, May 1966.

[8] R.F.Harrington, *Field Computation by the Moment Method*. New York:MacMillan, 1968.

[9] A.M. van de Water, B.P. de Hon, M.C. van Beurden, A.G. Tijhuis, and P. de Maagt, "Linear embedding via green's operators: A modeling technique for finite electromagnetic band-gap structures," *Physical Review E*, vol. 72, Nov. 2005.

[10] G.Krohn, "A set of principles to interconnect the solutions of physical systems," *Journal of Applied Physics*, vol. 24, pp. 965–980, Aug. 1953.

[11] V.Lancellotti, B.P. de Hon, and A.G.Tijhuis, "An eigencurrent approach to the analysis of electrically large 3-D structures using LEGO," *IEEE Trans. Antennas Propagat.*, vol. 57, pp. 3575–3585, Nov. 2009.

[12] G. Goubau, N.N. Puri, and F. Schwering, "Diakoptic theory of multielements antennas," *IEEE Trans. Antennas Propagat.*, vol. 30, pp. 15–26, Jan. 1982.

[13] F. Schwering, N.N.Puri, and C.M. Butler, "Modified diakoptic theory of antennas," *IEEE Trans. Antennas Propagat.*, vol. 34, pp. 1273–1281, Nov. 1986.

[14] S.R. Rengarajan and Y.R Samii, "The field equivalence principle: Illustration of the estabishment of the non-intituive null fields," *IEEE Trans. Antennas Propagat.*, vol. 42, pp. 122–128, Aug. 2000.

[15] C.P Davis and K.F Warnick, "High-order convergence with a low order discretization of the 2-d MFIE," *IEEE Antennas Wireless Propagat. Lett.*, vol. 3, pp. 355–358, 2004.

[16] A.F. Peterson, S.L. Ray, and R. Mittra, *Computational Methods for Electromagnetics*. Piscataway: IEEE Press, 1998.

[17] P.Yla-Oijala and M. Taskinen, "Well-conditioned Müller formulation for electromagnetic scattering by dielectric objects," *IEEE Trans. Antennas Propagat.*, vol. 53, pp. 3316–3323, Oct. 2005.

[18] H.Boutayeb, T.A Denidni, K. Mahdjoudi, A.C Tarot, A.R Sebak, and L. Talbi, "Analysis and design of a cylindrical ebg-based directive antenna," *IEEE Trans. Antennas Propagat.*, vol. 54, pp. 211–219, Jan. 2006.

[19] H. Boutayeb, A.C Tarot, and K. Mahdjoudi, "Focusing characteristics of a metallic cylindrical electromagnetic band-gap structure with defects," *Progress In Electromagnetics Research*, vol. 66, pp. 89–103, 2006.